AEDC-TR-85-37

Robert Hess

UNCLASSIFIED

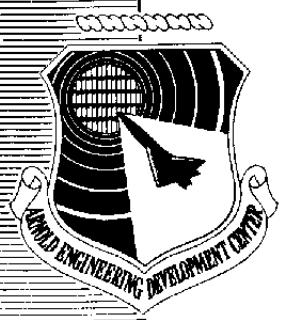




# High-Resolution Tunable Diode Laser Spectroscopy of Methane

H. C. Walker, Jr. and W. J. Phillips
Sverdrup Technology, Inc.

March 1986

Final Report for Period October 1, 1981 – September 30, 1983

Approved for public release; distribution unlimited.

**ARNOLD ENGINEERING DEVELOPMENT CENTER**
**ARNOLD AIR FORCE STATION, TENNESSEE**
**AIR FORCE SYSTEMS COMMAND**
**UNITED STATES AIR FORCE**

## NOTICES

When U. S. Government drawings, specifications, or other data are used for any purpose other than a definitely related Government procurement operation, the Government thereby incurs no responsibility nor any obligation whatsoever, and the fact that the government may have formulated, furnished, or in any way supplied the said drawings, specifications, or other data, is not to be regarded by implication or otherwise, or in any manner licensing the holder or any other person or corporation, or conveying any rights or permission to manufacture, use, or sell any patented invention that may in any way be related thereto.

Qualified users may obtain copies of this report from the Defense Technical Information Center.

References to named commercial products in this report are not to be considered in any sense as an endorsement of the product by the United States Air Force or the Government.

This report has been reviewed by the Office of Public Affairs (PA) and is releasable to the National Technical Information Service (NTIS). At NTIS, it will be available to the general public, including foreign nations.

**APPROVAL STATEMENT**

This report has been reviewed and approved.

Frank T. Tanji

FRANK T. TANJI, Captain, USAF
Directorate of Technology
Deputy for Operations

Approved for publication:

FOR THE COMMANDER

Lowell C. Keel

LOWELL C. KEEL, Lt Colonel, USAF
Director of Technology
Deputy for Operations

UNCLASSIFIED
SECURITY CLASSIFICATION OF THIS PAGE

## REPORT DOCUMENTATION PAGE

| | |
|---|---|
| 1a. REPORT SECURITY CLASSIFICATION<br>UNCLASSIFIED | 1b. RESTRICTIVE MARKINGS |
| 2a. SECURITY CLASSIFICATION AUTHORITY | 3. DISTRIBUTION/AVAILABILITY OF REPORT<br>Approved for public release; distribution unlimited. |
| 2b. DECLASSIFICATION/DOWNGRADING SCHEDULE | |
| 4. PERFORMING ORGANIZATION REPORT NUMBER(S)<br>AEDC-TR-85-37 | 5. MONITORING ORGANIZATION REPORT NUMBER(S) |
| 6a. NAME OF PERFORMING ORGANIZATION<br>Arnold Engineering Development Center<br>6b. OFFICE SYMBOL (If applicable)<br>DOT | 7a. NAME OF MONITORING ORGANIZATION |
| 6c. ADDRESS (City, State and ZIP Code)<br>Air Force Systems Command<br>Arnold Air Force Station, TN 37389-5000 | 7b. ADDRESS (City, State and ZIP Code) |
| 8a. NAME OF FUNDING/SPONSORING ORGANIZATION<br>Arnold Engineering Development Center<br>8b. OFFICE SYMBOL (If applicable)<br>DO | 9. PROCUREMENT INSTRUMENT IDENTIFICATION NUMBER |
| 8c. ADDRESS (City, State and ZIP Code)<br>Air Force Systems Command<br>Arnold Air Force Station, TN 37389-5000 | 10. SOURCE OF FUNDING NOS.<br>PROGRAM ELEMENT NO: 65807F<br>PROJECT NO: D239<br>TASK NO.<br>WORK UNIT NO. |
| 11. TITLE (Include Security Classification)<br>PLEASE SEE REVERSE OF THIS PAGE | |
| 12. PERSONAL AUTHOR(S)<br>Walker, H. C., Jr. and Phillips, W. J., Sverdrup Technology, Inc., AEDC Group | |
| 13a. TYPE OF REPORT<br>Final<br>13b. TIME COVERED<br>FROM 10/1/81 TO 9/30/83 | 14. DATE OF REPORT (Yr., Mo., Day)<br>March 1986<br>15. PAGE COUNT<br>48 |
| 16. SUPPLEMENTARY NOTATION<br>Available in Defense Technical Information Center (DTIC). | |

| 17 COSATI CODES | | | 18. SUBJECT TERMS (Continue on reverse if necessary and identify by block number) | | | |
|---|---|---|---|---|---|---|
| FIELD | GROUP | SUB GR | | | | |
| 07 | 04 | | methane | spectroscopy | infrared | tunable |
| 21 | 05 | | hydrocarbon | line width | turbojet | diode |
| | | | exhaust | pressure broadening | gas generator | laser |

19. ABSTRACT (Continue on reverse if necessary and identify by block number)

The feasibility of using tunable diode laser spectroscopy for measurement of methane concentration in turbine engine exhausts was investigated. An experimental program was accomplished in which the foreign gas broadening parameters of the methane R(0)A line of the $\nu_3$ fundamental band were measured for nitrogen and carbon dioxide broadening. The temperature range was extended from the room temperature data available in the literature to 1000K, typical of turbine engine exhausts. The range of concentrations and path lengths over which the technique is feasible was established. A literature survey on typical turbine engine emissions was conducted from which it was determined that the technique may be applicable at augmented power settings, but methane concentrations are too small for idle and intermediate power settings.

| | |
|---|---|
| 20. DISTRIBUTION/AVAILABILITY OF ABSTRACT<br>UNCLASSIFIED/UNLIMITED ☐ SAME AS RPT ☒ DTIC USERS ☐ | 21 ABSTRACT SECURITY CLASSIFICATION<br>UNCLASSIFIED |
| 22a. NAME OF RESPONSIBLE INDIVIDUAL<br>W. O. Cole | 22b TELEPHONE NUMBER (Include Area Code)<br>(615) 454-7813<br>22c OFFICE SYMBOL<br>DOS |

DD FORM 1473, 83 APR EDITION OF 1 JAN 73 IS OBSOLETE

UNCLASSIFIED
SECURITY CLASSIFICATION OF THIS PAGE

11. TITLE

High-Resolution Tunable Diode Laser Spectroscopy of Methane

## PREFACE

The work reported herein was conducted by the Arnold Engineering Development Center (AEDC), Air Force System Command (AFSC), under Program Element 65807F. The results were obtained under Sverdrup Project No. D239 by Sverdrup Technology, Inc., AEDC Group, operating contractor for the Engine Test Facilities at AEDC , AFSC, Arnold Air Force Station, Tennessee. The Air Force Project Managers were Lt. S. W. Lehr and Capt. F. T. Tanji. The manuscript was submitted for publication on April 2, 1985.

## CONTENTS



## ILLUSTRATIONS



## TABLES



## APPENDIX

# 1.0 INTRODUCTION

A renewed interest in combustion mechanisms has been brought about by the increasing demands for efficiency and power placed on combustion systems. Several new diagnostic techniques are being developed to study combustion through quantitative measurements of the combustion products. Nonintrusive methods of measuring concentration and temperature of specific molecules in the exhaust streams of rocket and turbine engines are being sought to replace the probe methods currently being used. The probe methods provide results which are subject to question as the probe itself may chemically alter the exhaust gas which is drawn off for analysis with commercial gas analysers (Refs. 1-5). One technique being developed at Arnold Engineering Development Center (AEDC) as a possible replacement for the probes is tunable diode laser (TDL) absorption spectroscopy. In support of this technique, laboratory measurements are being conducted on molecules of interest in combustion flows.

A class of molecular emissions of great interest from aircraft engines is hydrocarbons, since most fuels are hydrocarbon based. Commercial gas analyzers usually provide total hydrocarbon counts in methane equivalents rather than concentrations of specific species of hydrocarbons. For many purposes this is sufficient; however, a knowledge of specific hydrocarbon concentrations may be necessary for combustion system chemical kinetics studies, computer code validation, and pollutant emissions definition. The concentration of exhaust constituents attributable to complete combustion and incomplete combustion would also be of importance to validation of the engine design.

TDL measurements can be made by passing the laser beam through the exhaust gases as they exit the engine. The energy absorbed from the laser beam at a tuned wavelength is related to species concentration; that is, the absorption coefficient is proportional to the number of absorbing molecules in the beam. The absorption coefficient depends on wavelength (line shape), as well as a line strength function, which is temperature dependent. The line shape is affected by collisions of all molecular species in the gas with the absorbing molecules; therefore, the absorption is a function of the partial pressure of each gas present. Each gas present has a characteristic effect on the shape of the absorption line.

The TDL has a line width on the order of $10^{-4}$ wave numbers. This provides sufficient resolution to determine the true line shape since most absorption lines in the 2 - 5 $\mu$m IR spectral region have a full width at half maximum (FWHM) of 0.1 to 0.2 wave numbers. Additionally, the TDL can be used to determine the exhaust gas temperature by the two-line technique for certain well-defined species. This technique makes use of the temperature dependence of the line strength function.

Laboratory measurements of methane, a principal component of most hydrocarbon combustors, were made to determine if TDL absorption spectroscopy is a reasonable approach to quantitative measurements. These measurements were made on the R(0) absorption line of the $\nu_3$ vibrational band of methane with a center frequency of 3028.75 $cm^{-1}$. This is the C-H stretch band present in many hydrocarbon molecules in addition to methane. Therefore, much of the work here should be applicable to other hydrocarbon species. This line was chosen because it has a single symmetry component which makes the analysis more tractable. In addition, this line appears to be free from interference by other species which are expected to be among the combustion products.

To determine concentration or temperature from absorption spectroscopy, the line parameters (i.e., line strength and collisional broadening half width) must be known. The line strength has been measured (Ref. 6). However, the collision-(or Lorentz) broadening parameters for methane broadened by nitrogen have previously been reported only in the temperature range from 100 to 300 K (Refs. 6 and 7). Measurements have not been reported at higher temperatures in the range appropriate to turbine engine exhausts. This work presents measured collison-broadening parameters of methane broadened by nitrogen and carbon dioxide as a function of temperature in the range from 300 to 1000 K, with determination of the temperature dependence for extrapolation to higher temperature.

A literature study was conducted (Appendix A) to determine which unburned hydrocarbons are most abundant in turbine engine exhausts. Based upon this study, methane appears to be a major constituent of the hydrocarbons in turbine engine exhausts for some, but not all cases. Calculations were undertaken to assess the ability of the TDL to make methane concentration measurements on exhaust plumes typical of turbine engines.

## 2.0 THEORY

### 2.1 LINE ABSORPTION

The theoretical development of quantitative molecular spectroscopy was accomplished far in advance of the development of spectrometers of sufficient resolution to take full advantage of the theory. With the use of high resolution laser spectrometers (the TDL has a resolution on the order of $10^{-4}$ wave numbers), the theory can be used without the approximations required by less accurate instrumentation. Therefore, the measured TDL absorption line profiles can be analyzed within the framework of well-established theory (Refs. 8, 9, and 10). For transmission of monochromatic radiation through a homogeneous gas path, the transmitted radiation is related to the incident radiation by the Lambert-Beers law:

$$I(\omega) = I^{o}(\omega) \exp(-k(\omega)\ell) \tag{1}$$

where

| | | |
|---|---|---|
| $I(\omega)$ | = | Spectral intensity transmitted by sample at frequency $\omega$ |
| $I^{o}(\omega)$ | = | Incident spectral intensity at frequency $\omega$ |
| $k(\omega)$ | = | Absorption coefficient at frequency $\omega$ |
| $\ell$ | = | Path length |
| $\omega$ | = | Frequency of radiation in wave numbers ($cm^{-1}$) |

At very high resolution such as with the TDL spectrometer, the true line shape will be obtained from a transmission measurement by tuning the laser through a frequency range including the absorption line. The line strength, S, is defined for an isolated absorption line by the equation:

$$S = S_{o}^{J''-J'} P = \int_{-\infty}^{\infty} k(\omega)\, d\omega \tag{2}$$

where

| | | |
|---|---|---|
| $S_{o}^{J''-J'}$ | = | is the calculated absorption line strength ( $cm^{-2}-atm^{-1}$) |
| J | = | Rotational quantum number |
| $''$,$'$ | = | Indicates lower and upper states, respectively |
| P | = | Partial pressure of absorber (atm) |

The line strength at a given temperature can be calculated for a given transition by the following equation (Ref. 11):

$$S_{o}^{J'',J'} = \frac{8\pi^{3}}{3hc} \underbrace{\omega}_{\text{line position}} \underbrace{\langle \mu \rangle^{2}}_{\text{dipole moment matrix element}} \underbrace{\frac{Ng_{J} \exp(-E_{J}^{V'',J''}/kT)}{Q_{V}^{(J)} Q_{R}^{(J)}}}_{\text{number of molecules in state } v'', J''} \underbrace{\left(1 - \exp(-\omega hc/kT)\right)}_{\text{stimulated emission term}} \tag{3}$$

where

| | | |
|---|---|---|
| h | = | Planck's constant (erg-sec) |
| c | = | Velocity of light in vacuum (cm/sec) |
| $<\mu>$ | = | Dipole moment matrix element ($cm^2$ esu-cm) |
| N | = | Total number of molecules ( $/cm^3$) |
| $g_J$ | = | Statistical weight including nuclear spin of the rotational energy state |
| $E_{J'}^{V''}$ | = | Lower state energy (erg) |
| k | = | Boltzmann's constant (erg/K) |
| T | = | Temperature (K) |
| $Q_V(T)$ | = | Vibrational partition function |
| $Q_R(T)$ | = | Rotational partition function |

The total number of molecules per cubic centimeter, N, can be written:

$$N = P \frac{T_o}{T} L \tag{4}$$

where

$\ell$ = Loschmidt's number ($mol/cm^3$-atm at STP)

The dipole moment matrix element can be broken into two parts,

$$<\mu>^2_{V'',V',J'',J'} = <\mu>^2_{J'',J'} \; F_V(M) \; <\mu>^2_{V'',V'} \tag{5}$$

where

| | | |
|---|---|---|
| $<\mu>_{J'',J'}$ | = | Rotation matrix element of the dipole moment |
| $F_V(M)$ | = | Accounts for vibration-rotation interaction effects (can be set equal to 1 with an error on the order of 5 percent |
| $\|M\|$ | = | J'' + 1 for the R branch, J'' for the P branch |

Then

$$S_o^{J'',J'} = \frac{8\pi^3}{3hc} \omega <\mu>^2_{J'',J'} \; F_V(M) P \frac{T_o}{T} \ell \frac{g_J \exp(-E_J^{V''}/kT)}{Q_V(1) \; Q_R(T)} (1 - \exp(-\omega hc/kT)) \tag{6}$$

A vibration band strength ($S^{o}_{V'',V'}$) can be defined such that

$$S^{o}_{V'',V'} = \frac{8\pi^3}{3hc}\,\omega_o <\mu>^2_{V'',V'} \frac{T_o}{T} \frac{e^{\frac{-E_{V''}}{kT}}}{Q_v(T)} \tag{7}$$

where

$\omega_o$ = frequency at the band center ($cm^{-1}$)

Then the line strength can be written in terms of the band strength.

$$S_o^{J'',J'} = S^{o}_{V'',V'} \frac{\omega}{\omega_o} P \frac{g_J e^{\frac{-E^{J''}}{kT}}}{Q_R(T)} \left( . - e^{\frac{-\omega hc}{kT}} \right) F_v(M) <\mu>^2_{J'',J'} \tag{8}$$

The rotational partition function can be calculated from the following equation:

$$Q_R(T) = \sum_{J''=0}^{\infty} g_{J''} \exp\left(-E_{J''}/kT\right) \tag{9}$$

To determine the absorption coefficient, the line shape function as well as the line strength is necessary. The parameter to be determined which specifies the line shape function is the half-width ($\gamma$). This parameter is defined as one-half of the width of the absorption coefficient curve at half maximum (HWHM). There are two limiting cases to be considered, corresponding to low pressure and high pressure. The Doppler function gives the line shape in the low pressure limiting case of no collisional broadening:

$$k(\omega) = \left( \frac{\ln 2}{\pi} \right)^{1/2} (S/\gamma_D) \exp\left( \frac{(\omega-\omega_0)^2 \ln^2}{\gamma_D^2} \right) \tag{10}$$

where the Doppler width is given by:

$$\gamma_D = \left( \frac{2kT \ln 2}{MC^2} \right)^{1/2} \omega_o \tag{11}$$

where M is the mass of the absorbing molecule. The Lorentzian function gives the line shape in the high pressure limiting case where collision broadening is dominant:

$$k(\omega) = \left( \frac{S}{\pi} \right) \frac{\gamma_L}{((\omega-\omega_0)^2 + \gamma_L^2)} \tag{12}$$

where $\gamma_L$ is the Lorentz half-width. Most measurements will fall between the two limiting pressures and can be covered by a general equation known as the Voigt line shape:

$$k(\omega) = S \left( \frac{(\ln 2/\pi)}{\gamma_D} \right) \frac{a}{\pi} \int_{-\infty}^{\infty} \frac{\exp(-y^2)}{a^2 + (x-y)^2} dy \tag{13}$$

where a is the Voigt parameter:

$$a = (\ln 2)^{1/2} \frac{\gamma_L}{\gamma_D} \tag{14}$$

$$x = (\omega - \omega_o)(\ln 2)^{1/2}/\gamma_D \tag{15}$$

is the normalized distance from line center frequency.

Pressure broadening is attributable to self broadening and foreign gas broadening. Self broadening is due to collisions with like molecules, while foreign gas broadening is due to collisions with other species present in the mixture. The absorption coefficient curve can be characterized by the parameter $\gamma_L^o$ ($cm^{-1}$-$atm^{-1}$), which is the collisional or Lorentz half-width attributable to broadening of the absorbing molecule by the foreign gas at 1 atm pressure. For the case of several foreign gases present, the Lorentz half-width is calculated by:

$$\gamma_l = \sum_i \gamma_{L_i}^o P_i \tag{16}$$

The $P_i$ and $\gamma_{L_i}^o$ are the partial pressure and Lorentz half-width at standard conditions for the ith foreign gas present in the mixture.

The Lorentz HWHM also contains a temperature dependence through the broadening parameters, $\gamma_{L_i}^o$, which can be approximated by means of the semi-empirical formula (Ref. 12):

$$\gamma_{L_i}(T) = \gamma_{L_i}(T_o) \left(\frac{T}{T_o}\right)^{-N_i} \tag{17}$$

where $\gamma_{L_i}^o(T_o)$ is usually given at the standard temperature 273.15 K and is the HWHM of the molecular absorption at atmospheric pressure. The temperature dependence exponent, $N_i$, allows the calculation of $\gamma_{L_i}^o(T)$ from $\gamma_{L_i}^o(To)$ for broadening species i. The results of the experimental work can be presented as a foreign gas broadening parameter and a

temperature dependence exponent which are characteristic of the particular foreign gas used to broaden a spectral line of the species of interest.

To compare line strengths for the same line but at different temperatures, an equation relating $S_o(T_1)$ to $S_o(T_2$ where $T_2$ is some reference temperature can be obtained by dividing $S_o(T_1)$ by $S_o(T_2)$ in Eq. (8):

$$\frac{S_o(T_1)}{S_o(T_2)} = \frac{T_2}{T_1}\frac{Q_v(T_2)Q_R(T_2)}{Q_v(T_1)Q_R(T_1)}\exp\left(\frac{E^{v''}}{k(\frac{1}{T_1}-\frac{1}{T_2})}\right)\exp\left(\frac{-E^{J''}}{k(\frac{1}{T_1}-\frac{1}{T_2})}\right)\frac{1-e^{\frac{-\omega hc}{kT_1}}}{1-e^{\frac{-\omega hc}{kT_2}}} \quad (18)$$

The concentration, or partial pressure, of the absorbing molecule can then be obtained from Eq. (2).

## 2.2 METHANE $\nu_3$ STRUCTURE

The $CH_4$ molecule is tetrahedral molecule and belongs to the $T_d$ point group (Ref. 10). The molecular vibrational modes of $CH_4$ are classified by the five symmetry species, of the $T_d$ point group, $A_1$, $A_2$, E, $F_1$, and $F_2$. The $A_1$ and $A_2$ species are the nondegenerate, totally symmetric representations of which the ground vibrational state belongs. Species E is doubly degenerate and the two F species, $F_1$ and $F_2$, are triply degenerate. Since the dipole moment in the $T_d$ point group arises from species $F_2$, the fundamental bands are also of species $F_2$.

Because of the Coriolis interaction, the three-fold degenerancy of the energy states of species $F_2$ is broken into three closely spaced energy states denoted $F_2^{(+)}$, $F_2^{(0)}$, and $F_2^{(-)}$. The selection rule for the vibrational symmetry species is given by

$$\begin{aligned} A \rightarrow F_2^{(-)} \quad & \Delta J = 1 \\ A \rightarrow F_2^{(0)} \quad & \Delta J = 0 \\ A \rightarrow F_2^{(+)} \quad & \Delta J = 1 \end{aligned}$$

and that of the rotational symmetry species:

$$\begin{aligned} A \rightarrow A \quad & \text{all } \Delta J \\ E \rightarrow E \quad & \text{all } \Delta J \\ F \rightarrow F \quad & \text{all } \Delta J \end{aligned}$$

Figure 1 illustrates the various transitions and energy levels associated with the $F_2^{(-)} \rightarrow A$ transition. Note that the R(0)A and R(1)F lines are the only ones shown which are singlet and isolated. The R(0)A line was within the tuning range of the diode laser on hand.

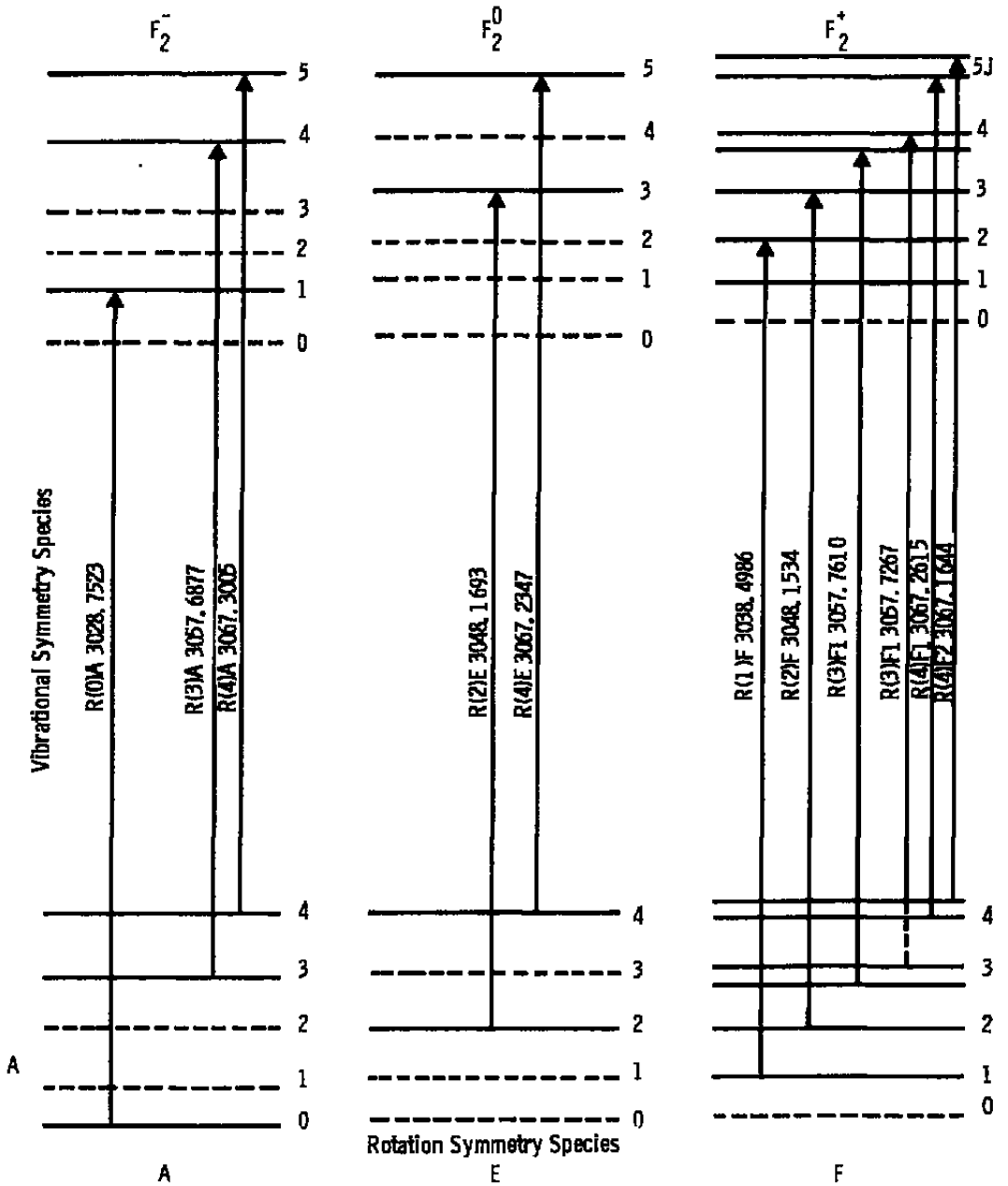


**Figure 1. Energy levels and transition diagram.**

## 3.0 EXPERIMENT

The absorption line shape data were taken using a Laser Analytics LS-3 high resolution tunable diode laser (TDL) absorption spectrometer. A schematic of the TDL absorption spectrometer system is shown in Fig. 2. The diode lasers, which are manufactured from single crystals grown from lead salt compounds, are contained in a temperature-controlled cold head which can be operated from 10 to 100°K. The diode lasers are obtained from Laser Analytics and have user specified tuning ranges of 10, 20, and 50 $cm^{-1}$. The diode lasers are tuned through this range by changing the temperature of the diode laser and the diode injection current. A 1°K change in temperature will cause a 4 $cm^{-1}$ change in laser output. When the diode laser output is tuned to the wave number of an absorption line by adjusting the cold head temperature, the laser output can be tuned across the line with Joule heating produced by modulating the diode injection current. The laser output contains several modes with a minimum multimode power of 0.1 mw. The line width of each mode is approximately $3 \times 10^{-4}$ $cm^{-1}$. The individual modes are typically 1 $cm^{-1}$ apart allowing a specific mode to be selected by use of a 0.5-m grating monochromator having a 0.5 $cm^{-1}$ resolution. Each mode can be tuned over a range of approximately 1 $cm^{-1}$.

The laser output is formed into a collimated beam by the f/1 collimating lens. A 3-in. slide mounted germanium etalon can be introduced into the collimated beam. The etalon produces fringes with a spacing of 0.0159 $cm^{-1}$ which are used to provide a precise wave number calibration of the laser beam.

The collimated beam is directed out of the TDL system through an absorption cell mounted in a furnace. The optical cell has sapphire windows bonded to Kovar flanges which are welded to the stainless steel absorption cell. The temperature of the gas in the absorption cell is monitored by a thermocouple inside the cell. The beam is subsequently directed through a calibration cell and back into the TDL system. Inside the TDL system is a 400-Hz tuning fork chopper and a 0.5-m grating monochromator. In addition to separating the laser modes, the monochromator provides a coarse (0.5 $cm^{-1}$) absolute wave number calibration. The tuning fork chopper, used in conjunction with a lock-in amplifier, increases the signal-to-noise ratio of the signal from the detector.

The output mirror of the monochromator focuses the beam on the entrance slits of the detector. The detector used in this work was a liquid nitrogen-cooled indium antimonide (InSb) detector. The peak responsivity for this detector is at 2080 $cm^{-1}$. The detector unit includes both adjustable optics for focusing the beam onto the 2 $mm^2$ active area of the detector, as well as an impedance matched pre- amplifier.

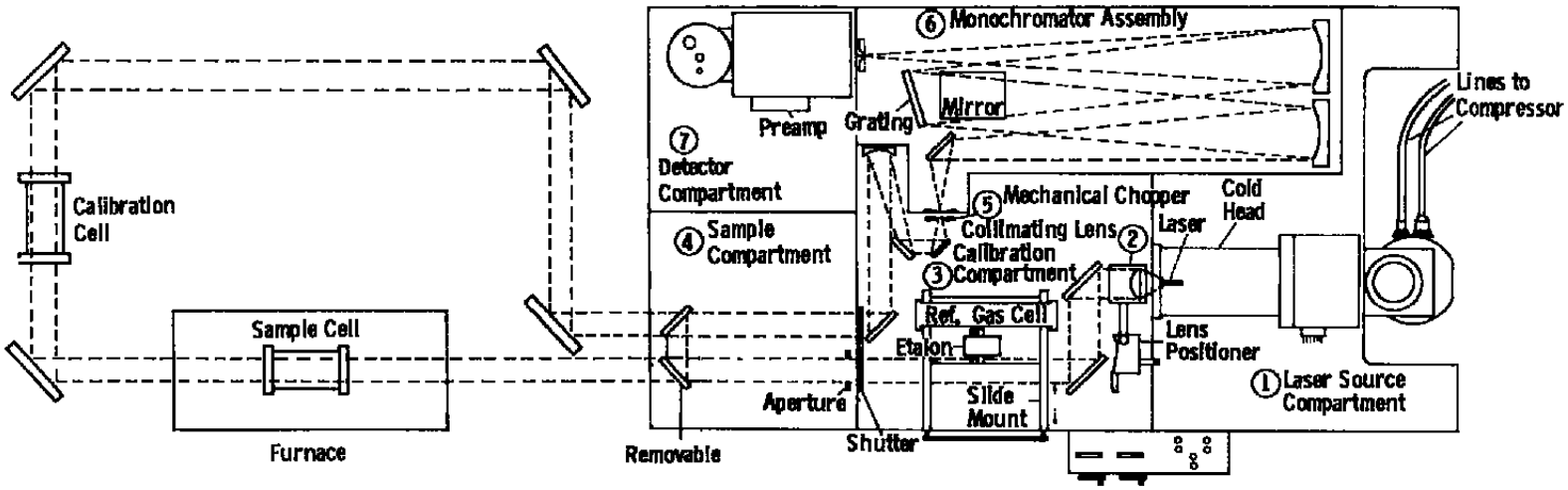


**Figure 2. Tunable diode laser absorption spectrometer.**

In the present work, measurements of the half width of the R(0)A absorption line of the $\nu_3$ vibrational band of methane at 3028.7523 $cm^{-1}$ were accomplished as a function of temperature and foreign gas pressure. The pressures used were 1/3, 2/3, and 1 atm, and the temperature range for the measurements was 300 to 1000 K.

## 4.0 METHANE CALIBRATION RESULTS

The equations presented in Section 2 were applied to the data obtained in this work to determine the effect of nitrogen and carbon dioxide on the spectral line shape of the R(0)A rotational line of the $\nu_3$ vibrational band of methane. The results are presented as a foreign gas broadening parameter which is characteristic of the particular foreign gas used to broaden the methane spectral line as a function of temperature and pressure. Also, the temperature dependence of $\nu_{Li}$ was presented as the exponent, $N_i$, in Eq. ( 17).

The broadening parameters at the various gas temperatures were obtained by performing a nonlinear least-square fit to the function given in Eq. (13) using the Voigt profile for the absorption coefficient and the spectral intensity profiles taken from the tunable diode laser spectrometer. The two fit parameters obtained are S and a of Eq. (13). S could not be determined absolutely because the concentration of methane in the samples was not accurately known. Dang Nhu, et al. (Ref. 13) give 2.3 $cm^{-2}atm^{-1}$ as a value of $S_o$ at standard conditions. The collision broadening parameter $\gamma_i^o$ is obtained from the Voigt parameter by the use of Eq. (14). From $\gamma_L$, measured pressure, measured temperature, the self broadening parameters and the use of Eq. (16), $\gamma_{N2}$ (T) (the foreign gas broadening parameter) was obtained. The temperature dependent foreign gas broadening parameters were then least-square fitted to Eq. (17) to obtain the foreign gas broadening parameters at standard temperature and to determine the temperature exponent, $N_i$.

The self broadening parameters which account for broadening attributable to collisions between methane molecules at the various temperatures used in the data analysis were obtained from the use of Eq. (17) and the self broadening data from Darnton and Margolis (Ref. 7) and Varanasi, et al. (Ref. 14) on the R(0) line of the $\nu_3$ and $2\nu_3$ vibrational bands (see Table 1). The data from both sources were combined and used to obtain a self broadening parameter of 0.0882 $cm^{-1}$-$atm^{-1}$ at 273.16 K with a temperature dependence exponent of -0.8339. Table 1 shows that all measurements of the self broadening were made in the temperature range of 82 to 298 K. The results obtained from Ref. 7 and Ref. 14, along with Eq. (17) were used to determine the self broadening at the temperatures investigated in the present work. It should be noted that the measurements made here are on the $\nu_3$ band, but according to the Anderson-Tsao-Curnutte broadening theory (Refs. 15-16) there should be little change in the half widths with respect to vibrational quantum number.

**Table 1. Half Width of the R(0) A Line for Methane Self Broadening.**

| Temp., °K | $CH_4$-$CH_4$($cm^{-1}$-$atm^{-1}$) | |
|---|---|---|
| | Ref. 7 | Ref. 14 |
| 82 | --- | 0.25 ± 0.02 |
| 100 | --- | 0.20 ± 0.02 |
| 130 | --- | 0.16 ± 0.01 |
| 160 | --- | 0.13 ± 0.01 |
| 190 | --- | 0.13 ± 0.01 |
| 211 | 0.1083 ± 0.0015 | --- |
| 250 | --- | 0.104 ± 0.009 |
| 295 | --- | 0.080 ± 0.07 |
| 298 | 0.0865 ± 0.0070 | --- |

Figure 3 shows typical data from the TDL absorption experiment which consist of a measurement with the cell evacuated, a measurement with the gas present, and the etalon measurement for wave number calibration. The transmission with the sample cell evacuated gives the amount of radiation transmitted from the diode laser through the optical system to the detector without the gas sample present in the beam path. The transmission with the gas present shows the amount of radiation which is transmitted through the system when the optical cell is filled with the absorbing gas. The difference between the two curves gives the amount of radiation absorbed by the gas sample. The transmission with the etalon is taken

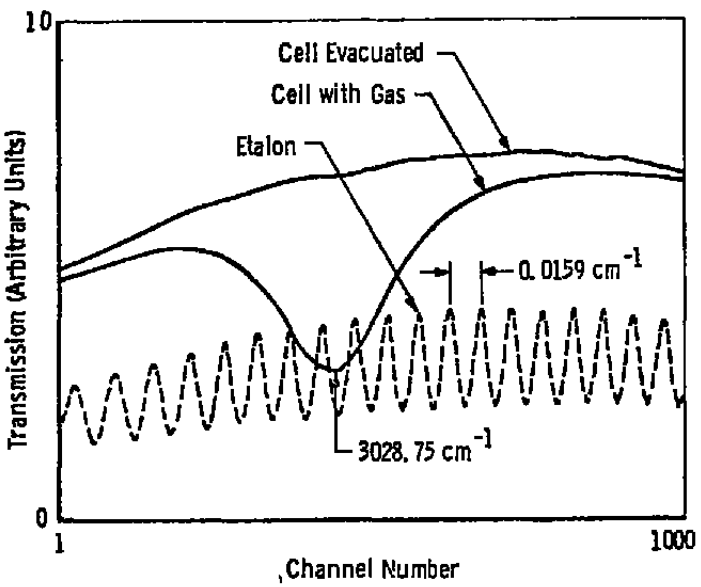


**Figure 3. Typical raw data from TDL for R(0) line of methane.**

with the optical cell evacuated and the germanium etalon in the beam. Adjacent peaks on the etalon transmission curve are 0.0159 $cm^{-1}$ apart; this allows the diode injection current to be related to the frequency in wave numbers.

Figure 4 shows the same data after analysis. The transmission with the cell evacuated has been smoothed and the Voigt profile which best fits the sample transmission curve has been calculated. As can be seen, the fit between the Voigt profile and the sample transmission is very good for this data . The foreign gas broadening parameters are obtained from these data to make the Voigt profile [Eq. (13)] fit the sample transmission. The data shown are for approximately 1/3 atm total pressure of methane and 2/3 atm carbon dioxide at 299 K. The fit to a Voigt profile yielded a value for the collision broadening parameter of 0.027 $cm^{-1}$-$atm^{-1}$.

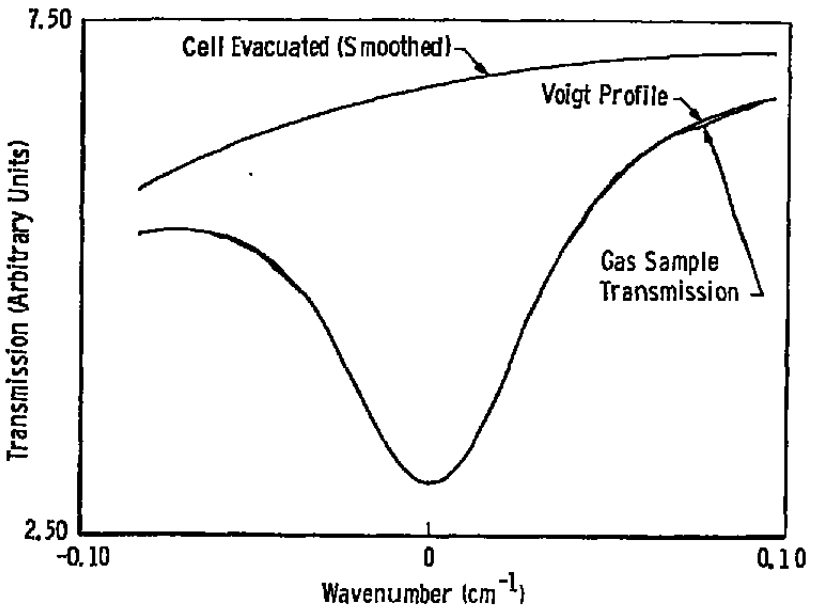


**Figure 4. Data from TDL for the R(0) line of methane.**

Over 200 data sets were taken with methane/nitrogen mixtures at pressures of approximately 1/3, 2/3 and 1 atm, and temperature increments of 100 K from 300 to 1000 K. The mean value of $\gamma_L^o$ (T) (HWHM) as a function of pressure for several representative temperatures is shown in Fig. 5. Theory predicts a linear relationship between $\gamma_L^o$ (T) and pressure which is observed in Fig. 5. The broadening parameter attributable to carbon dioxide collisons is shown in a similar way in Fig. 6. The results are given in tabular from for both gas mixtures in Table 2.

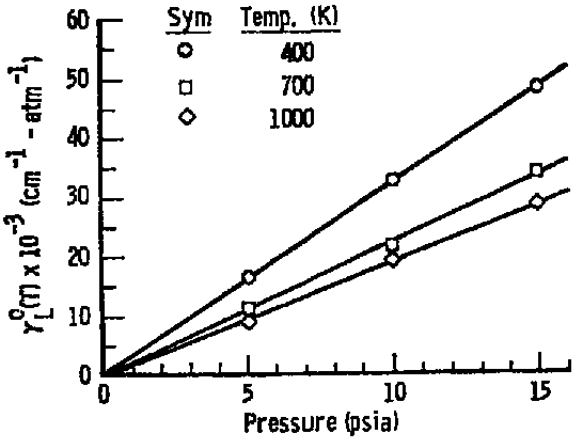


**Figure 5. Half width versus pressure for nitrogen broadening of methane.**

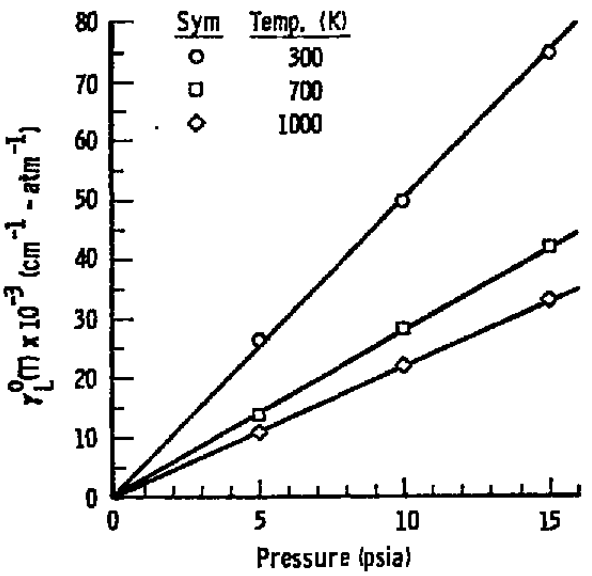


**Figure 6. Half width versus pressure for carbon dioxide broadening of methane.**

The collision broadening half width, $\gamma_L^o$, is the value for standard conditions which is calculated from the experimental values measured in this experiment. The nitrogen broadening of methane resulted in a $\gamma_L^o$ ($T_o$) of 0.05848 ± 0.00070 cm$^{-1}$-atm$^{-1}$ while the carbon dioxide broadening of methane results in a $\gamma_L^o$ ($T_o$) of 0.07874 ± 0.00011. The probable errors cited are one standard deviation of the data.

**Table 2. Summary of Results for Nitrogen and Carbon Dioxide Broadening of the $\nu_3$, R(0) Line of Methane**

| | $CH_4$ - $N_2$ | $CH_4$ - $CO_2$ |
|---|---|---|
| $T_o$(K) | 273.15 | 273.15 |
| $\gamma_L^o$ ($T_o$ ($cm^{-1}$-$atm^{-1}$) | 0.05848 ± 0.00070 | 0.07874 ± 0.00011 |
| $N_i$ | −0.6521 ± 0.0069 | −0.6881 ± 0.0029 |
| Standard Deviation | 0.0016 | 0.0016 |
| Total No. of Data Points | 224 | 96 |

The result that the carbon dioxide broadening parameter is greater than the nitrogen broadening parameter is consistent with theory since the carbon dioxide molecule has a dipole moment and nitrogen does not.

Darnton and Margolis (Ref. 7) measured the nitrogen broadening parameter for 100 and 298 K. The broadening parameter was calculated using Eq. (17) and the current results for these same temperatures and was found to be smaller than the values from Ref. 7. At 298 K the current measurements gave a value of 0.0553 ± 0.0003 $cm^{-1}$-$atm^{-1}$ versus 0.0590 ± 0.0067 $cm^{-1}$-$atm^{-1}$ from Ref. 7. The value given for the current measurements was obtained by extrapolating 2° beyond the lowest temperature measured through the use of Eq. (17) and should be quite good. Also, it is well within the probable error of the value from Ref. 7. The value obtained at 100 K was 0.1126 ± 0.0043 $cm^{-1}$-$atm^{-1}$ versus 0.1473 ± 0.0019 $cm^{-1}$-$atm^{-1}$ from Ref. 7. To obtain a value for 100 K, it was necessary to extrapolate using Eq. (17) 200° beyond the lowest temperature at which measurements were made in this work. Mehrotra and Boggs (Ref. 17) calculated the nitrogen broadening parameter for 300 and 100 K using the Murthy and Boggs theory. Their value at 300 K is 0.0529 $cm^{-1}$-$atm^{-1}$, which is somewhat lower than both experimental values. At 100 K they obtained a value of 0.1286 $cm^{-1}$-$atm^{-1}$, which falls between the current experimental value and the value measured by Darnton and Margolis.

The temperature exponents, $N_i$, obtained from fitting all of the experimental measurements to Eq. (17) are −0.6521 ± 0.0069 for nitrogen and −0.6881 ± 0.0029 for carbon dioxide. Darnton and Margolis obtained a temperature dependence exponent of −0.8379 ± 0.10 from their measurements using nitrogen, but their measurements were made at only two temperatures.

The average value of the collisional foreign gas broadening half width, $\gamma_i^o$, for each temperature measured is shown in Table 3.This value has been corrected for both Doppler broadening and methane self broadening. The probable error and total number of data points taken at each temperature are shown with each value of $\gamma_i^o$. As indicated by Eq. (17) the values of $\gamma_i^o$ from Table 3, when plotted against temperature on log-log paper, should yield a straight line. Figure 7 is a plot of the nitrogen broadening data. The points approximate a straight line very well in that a straight line can be drawn through the data which is within one standard deviation of all the points. Figure 8 is a plot of the carbon dioxide data with a similar good fit to a straight line.

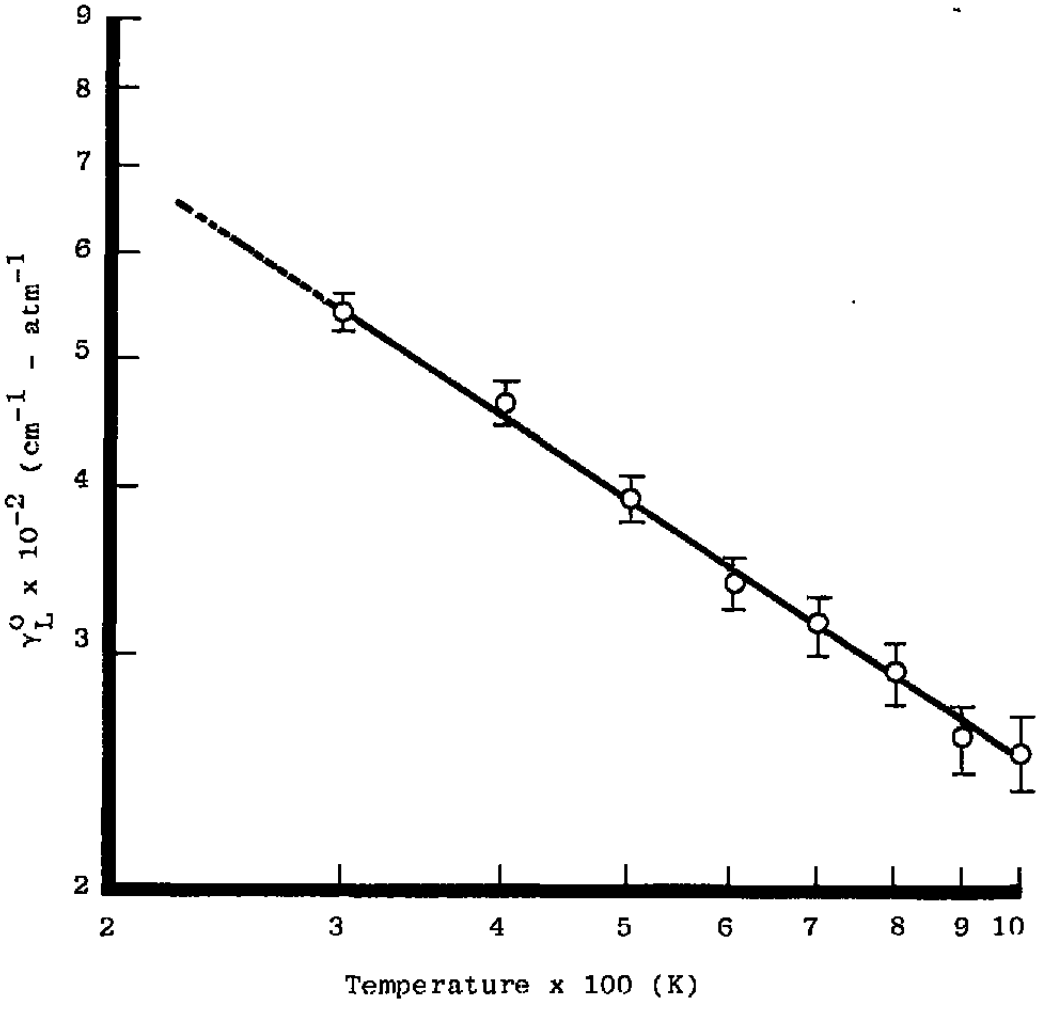


**Figure 7. Half width versus temperature for nitrogen broadening of methane.**

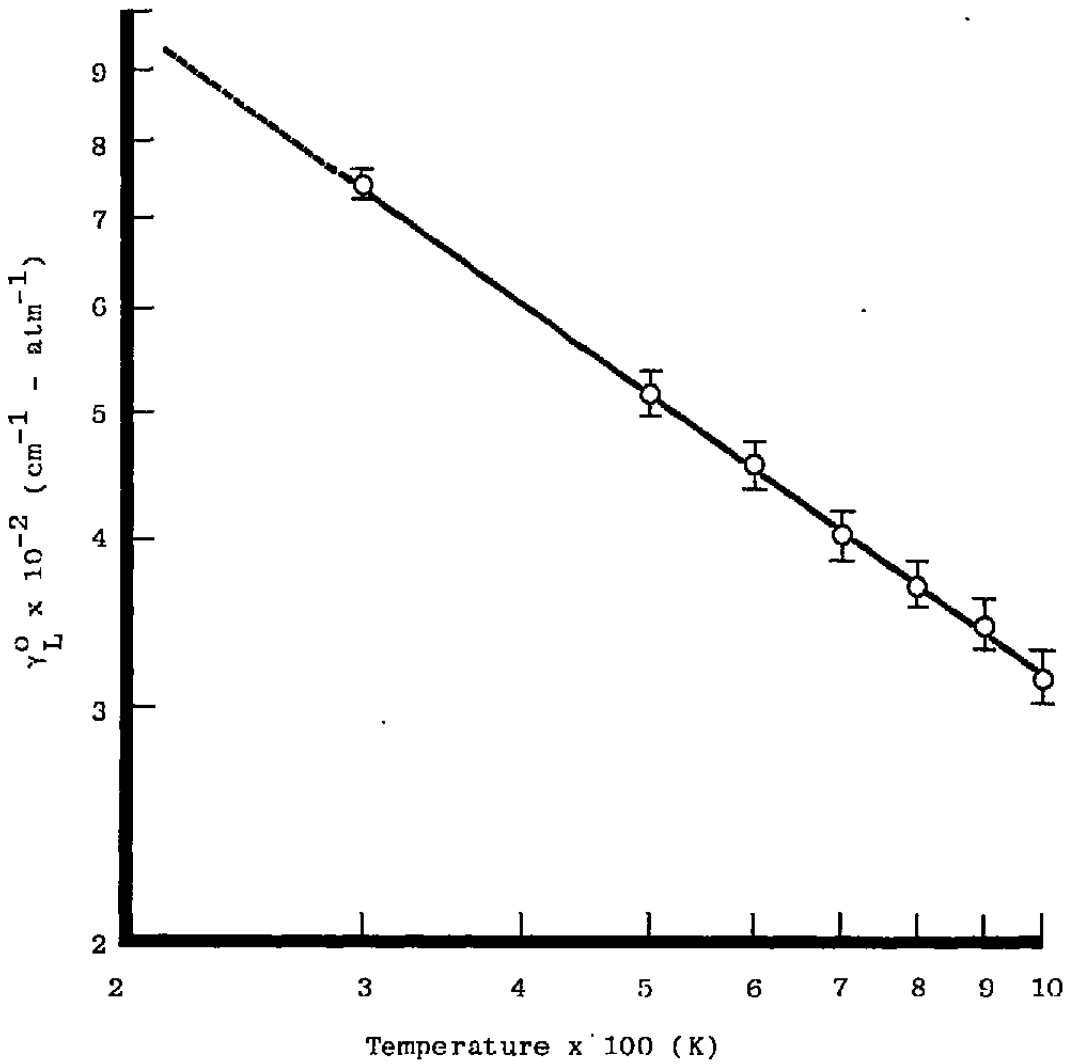


**Figure 8. Half width versus temperature for carbon dioxide broadening of methane.**

An error analysis was conducted on the data and the probable error in $\gamma_L$, shown in the data tables, was calculated for each data set. In addition to the error analysis on $\gamma_L$, calibration gases of methane and carbon dioxide were mixed and used at 300 and 400 K. The average line strength measured for 0.81-percent $CH_4$ in carbon dioxide at 300 K was 1.97 $cm^{-2}$-$atm^{-1}$ and for 2.09-percent $CH_4$ in carbon dioxide at 400 K was 1.02 $cm^{-2}$-$atm^{-1}$. At standard temperature these values are 2.16 and 1.49 $cm^{-2}$ $atm^{-1}$, respectively, compared to 2.3 $cm^{-2}atm^{-1}$ obtained by Dang-Nhu et al. (Ref. 13). The line strength obtained from the Voigt fit profiles was used in Eq. (2), along with a value of $S_o$ calculated from Eq. (8) to determine the partial pressure of methane in the calibration mixture at various temperatures. The deviation from the laboratory prepared mixture of the calculated partial pressures ranged from less than 1 percent to a maximum of 7 percent. Based on these two error

**Table 3. Average Half Widths for Nitrogen and Carbon Dioxide Broadening of the ($T_3$), R(0) Line of Methane as a Function of Temperature**

| Temp., (°K) | Average $\gamma$ $CH_4$-$N_2$ (T) ($cm^{-1}$-$atm^{-1}$) | No. of Data Points | Average $\gamma$ $CH_4$ - $CO_2$ (T) ($cm^{-1}$-$atm^{-1}$) | No. of Data Points |
|---|---|---|---|---|
| 300 | 0.05452 ± 0.00028 | 33 | 0.07413 ± 0.00059 | 10 |
| 400 | 0.04647 ± 0.00014 | 48 | --- | --- |
| 500 | 0.03946 ± 0.00015 | 30 | 0.05174 ± 0.00017 | 15 |
| 600 | 0.03421 ± 0.00013 | 41 | 0.04621 ± 0.00035 | 14 |
| 700 | 0.03203 ± 0.00020 | 15 | 0.04066 ± 0.00024 | 14 |
| 800 | 0.02947 ± 0.00020 | 18 | 0.03743 ± 0.00019 | 15 |
| 900 | 0.02617 ± 0.00013 | 18 | 0.03525 ± 0.00028 | 14 |
| 1000 | 0.02568 ± 0.00016 | 21 | 0.03214 ± 0.00017 | 14 |

analysis methods, it is estimated that the absolute error to be expected in a measurement of $CH_4$ concentration by the TDL method would be less than 7 percent. This really represents a check on the consistency of the theory rather than a calibration error. Direct calibration at a given temperature and pressure should yield errors consistent with other calibrated methods, about 2 percent.

## 5.0 METHANE CALCULATIONS BASED ON TDL SENSITIVITY

The range of concentration and path length suitable for TDL measurement of methane can be calculated, based on the line center absorption of the R (0) A line of the $\nu_3$ band. An approximation based on Eq. (12) at line center ($\omega = \omega_o$) was used for the absorption coefficient. This approximation and Eq. (1) gives the following equation for the transmission of radiation through the exhaust stream.

$$T(\omega_o) = \frac{I(\omega_o)}{I^o(\omega_o)} = \exp\left(-S_o \ell F / II\gamma_I^o\right)$$

$T(\omega_o)$ = transmittance

$F$ = mole fraction of absorber

$S_o$ = line strength, $cm^{-1}$-$atm^{-1}$, at temperature T

$\ell$ = path length, cm

The ideal case for measurements with the TDL absorption spectrometer would be to have 50- to 60-percent absorption at line center; however, measurements are possible with line center absorption in the range from 20-to 95-percent. Calculations were performed to

determine the required concentration of methane to give 20- and 95-percent absorption of radiation at line center as a function of path length through the exhaust. An exhaust gas temperature of 1000° K was assumed for the calculation. The results of the calculation are presented in Fig. 9. For methane concentrations between the two curves, TDL concentration measurements should be possible.

The methane concentrations and path lengths (exhaust nozzle diameter) obtained from the survey reported in Appendix A are summarized as follows:

| Engine | Exhaust Nozzle Diameter (in.) | Methane Concentration (ppmv) | | |
|---|---|---|---|---|
| | | Idle | Cruise | Afterburner |
| J85 | 18 | 18 | 0.5 | 130 - 240 |
| J93 | 30 | 20 | 2 | 90 - 180 |
| TF39 | 38 | 10 | 0.2 | --- |
| TF56 | 20 | 4 | 0.4 | --- |

Based on these data and Fig. 9, multiple reflections would be required to make measurements of methane concentration for any of these engines, even at augmented power setting.

## 6.0 SUMMARY

The purpose of this work was to determine if the TDL spectrometer could be used to measure the concentration of specific hydrocarbons in the exhaust of turbine engines. A literature survey was conducted to determine the hydrocarbon characteristics of turbine engines as a function of operating conditions. The results of this survey are presented in Appendix A. Based upon this survey, methane was found to be a constituent of the total hydrocarbons and data were found to define approximate concentration.

The R (0) line of the $\nu_3$ vibrational band of methane is a single line which is sufficiently isolated from other spectral lines in the band to permit measurements of the line profile. Laboratory measurements were made on this line of methane using a tunable diode laser (TDL) spectrometer. Since methane is of interest to astronomers, most measurements of methane molecular parameters are at room temperature or lower. In the current work measurements were made of pressure broadening parameters from 300 to 1000 K using carbon dioxide and nitrogen as broadening gases. The pressure broadening parameters are needed in making quantitative measurements with the TDL.

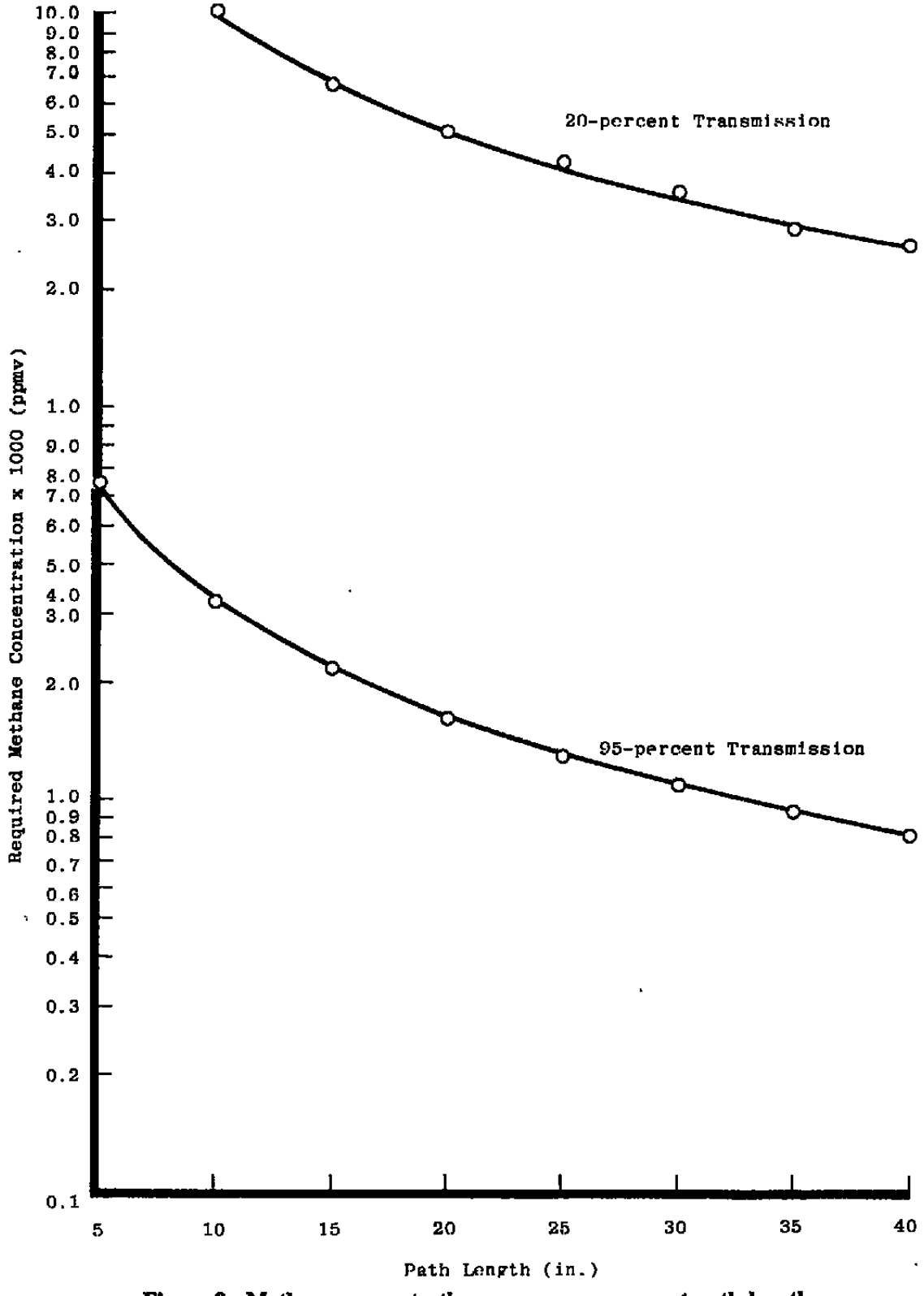


**Figure 9. Methane concentration versus measurement path length for 20- and 95-percent absorption.**

Using these results, calculations were performed to determine the range of methane concentrations over which TDL measurements should be possible. It was found that measurements of methane concentration are probably not possible on turbine engines at idle and cruise conditions. However, measurements may be possible for augmentor power conditions for large engine if multiple passes of the TDL beam are made.

## REFERENCES

1. Meinel, H., and Krauss, L. "Monitoring of Nitric Oxide in Flames by UV Differential Resonance Absorption." *Combustion and Flame,* Vol. 33, No. 1, September 1978, pp. 69 - 77.

2. Few, J. D. , Bryson, R. J. and McGregor, W. K. "Evaluation of Probe Sampling Versus Optical In-Situ Measurements of Nitric Oxide Concentrations in a Jet Engine Combustor Exhaust." AEDC-TR-76-180 (AD-A034726), January 1977.

3. Few, J. D. McGregor, W. K., and Glassman, H. N. "Comparison of UV Absorption Measurements with Probe-Sampling Measurements of Nitric Oxide Concentrations in a Jet Engine Combustor Exhaust." AEDC-TR-76-134 (AD-A030005), September 1976.

4. Benson, R. and Samuelson, G. S. "Oxides of Nitrogen Transformation While Sampling Combustion Products Containing Carbon Monoxide and Hydrogen." Combustion Institute Fall Meeting, La Jolla, California, October 18 - 20, 1976, Paper 76-39.

5. Benson, R. and Samuelson, G. S. "Oxide of Nitrogen Transformation While Sampling Combustion Products Containing Carbon Monoxide, Hydrogen, and Hydrocarbons." Combustion Institute Spring Meeting, Seattle, Washington, April 18 - 19, 1977, Paper 77-7.

6. Varanasi, P. "Collision-Broadened Half-Widths and Shapes of Methane Lines." *Journal of Quantitative Specroscopy and Radiative Transfer,* Vol. 11, No. 11, November 1971, p. 1711 - 1724.

7. Darnton, L. and Margolis, J. S. "The Temperature Dependence of the Half-Widths of Some Self-and Foreign-Gas-Broadened Lines of Methane." *Journal of Quantitative Spectroscopy and Radiative Transfer,* Vol. 13, No. 10, October 1973, p. 969 - 976.

8. Penner, S. S. *Quantitative Molecular Spectroscopy and Gas Emmissivities.* Addison-Wesley Publishing Company, Inc., Reading, Mass., 1959.

9. Thorne, A. P. *Spectrophysics.* Chapman and Hall, London, 1974.

10. Herzberg, G. *Molecular Spectra and Molecular Structure, II. Infrared and Raman Spectra of Polyatomic Molecules.* D. Van Nostrand, Inc., New York, 1966.

11. Fox, K. and Person, W. B. "Transition Moments in Infrared-active Fundamentals of Spherical-top Molecules." *Journal of Chemical Physics,* Vol. 64, No. 12, p. 5218, 1976.

12. Birnbaum, G. "Microwave Pressure Broadening." *Advances in Chemical Physics,* Vol. 12, 1967, p. 487.

13. Dang-Nhu, M., Pine, A. S., and Robiette, A. G. "Spectral Intensities in the $\nu_3$ Bands of $^{12}CH_4$ and $^{13}CH_4$." *Journal of Molecular Spectroscopy,* Vol. 77, 1979, pp. 57 - 68.

14. Varanasi, P., Sarangi, S., and Pugh L. "Measurements on the Infrared Lines of Planetary Gases at Low Temperatures. I. $\nu_3$ - Fundamental of Methane." *The Astrophysical Journal,* Vol. 179, No. 3, February 1973, pp. 977 - 982.

15. Taso, C. J. and Curnutte, B. "Line-Widths of Pressure-Broadened Spectral Lines." *Journal of Quantitative Spectroscopy and Radiative Transfer,* Vol. 2, p. 41, 1962.

16. Anderson, P. W. "Pressure Broadening in the Microwave and Infrared Regions." *Physics Review,* Vol. 76, No. 5, 1949, p. 647.

17. Mehrotra, S. C. and Boggs, J. E., "Calculation of the Self- and Foreign Gas-Broadened Widths of Rotational Lines in Vibrational Bands." *Indian Journal of Pure and Applied Physics,* Vol. 15, 1977, p. 764.

18. Grobman, J. "Review of Jet Engine Emissions." NASA TMX-68064, February 1972.

19. Lazalier, G. R. and Gearhart, J. W. "Measurement of Pollutant Emissions from an Afterburning Turbojet Engine at Ground Level II. Gaseous Emissions." AEDC-TR-72-70 (AD-747773), August 1972.

20. Davidson, D. L. and Domal, A. F. "Emission Measurements of A J93 Turbojet Engine." AEDC-TR-73-132 (AD-766648), September 1973.

21. Berry, D. A., Holdren, M. W., Lyon, T. F., Riggin, R. M. and Spicer, C. W. "Turbine Engine Exhaust Hydrocarbon Analysis Task 1 and 2." AF Engineering and Services Laboratory, Tyndall AFB, Florida, ESL-TR-82-43, June 1984.

22. Spicer, C. W., Holdren, M. W., Lyon, T. F. and Riggin, R. M. "Composition and Photochemical Reactivity of Turbine Engine Exhaust." AF Engineering and Services Laboratory, Tyndall AFB, Florida, ESL-TR-84-28, September 1984.

# APPENDIX A

## SURVEY TO DETERMINE EXHAUST CONSTITUENTS OF TURBINE ENGINES

The available data on turbine engine exhaust constituents were obtained by using sampling probes and gas analyzers. Although the probe techniques have come under suspicion, it will be assumed that their results are adequate for identifying the exhaust constituents. Before looking at the more detailed studies, the general relationships between exhaust constituents and turbine engine operating conditions will be presented. These relationships are based upon several studies (Ref. 18) and are generally true of all turbine engines, although not specific to a particular turbine engine.

### 1.0 OPERATING CHARACTERISTICS OF TURBINE ENGINE

The exhaust constituents from turbine engines depend on the operating conditions and their effect on the gas turbine combustor. There are five classes of constituents in the exhaust stream: products of complete combustion, products of incomplete combustion, unreacted air, oxides of nitrogen, and trace elements in the fuel. At takeoff and cruise conditions, the turbine engine operates at near 99-percent combustion efficiency and the relative amounts of the different classes of exhaust products are as follows. The trace elements are from sulfur and metals in the kerosene fuel and form the smallest amount of exhaust products. The unreacted air ($N_2$, $O_2$) accounts for greater than 93 percent by volume of the exhaust. The products of complete combustion ($H_2O$, $CO_2$) are estimated to account for 5.5 percent of the exhaust.

That leaves approximately 1 percent of the exhaust to be made up of the products of incomplete combustion (CO, unburned HC, partially oxidized HC, H2, and smoke) and the oxides of nitrogen. These results are shown in Table A-1.

Figure A-1, from Ref. 18, shows the typical engine exhaust emission characteristics for an engine with a pressure ratio of 13.4 and using JP-5 fuel. The plot shows the emission index (grams of specific combustion products per kilogram of fuel burned) versus the percent of maximum engine speed. As can be seen from the figure, the production of CO and unburned or partially burned hydrocarbons is highest at idle speed and drops off steadily to maximum engine speed.

At less efficient power settings than cruise and takeoff, such as idle or in augmented engines, the products of incomplete combustion will make up a larger part of the exhaust. The inefficient combustion near idle is attributable to the combustion inlet temperature and pressure being lower, low fuel flow rates which result in poor fuel atomization, and lean

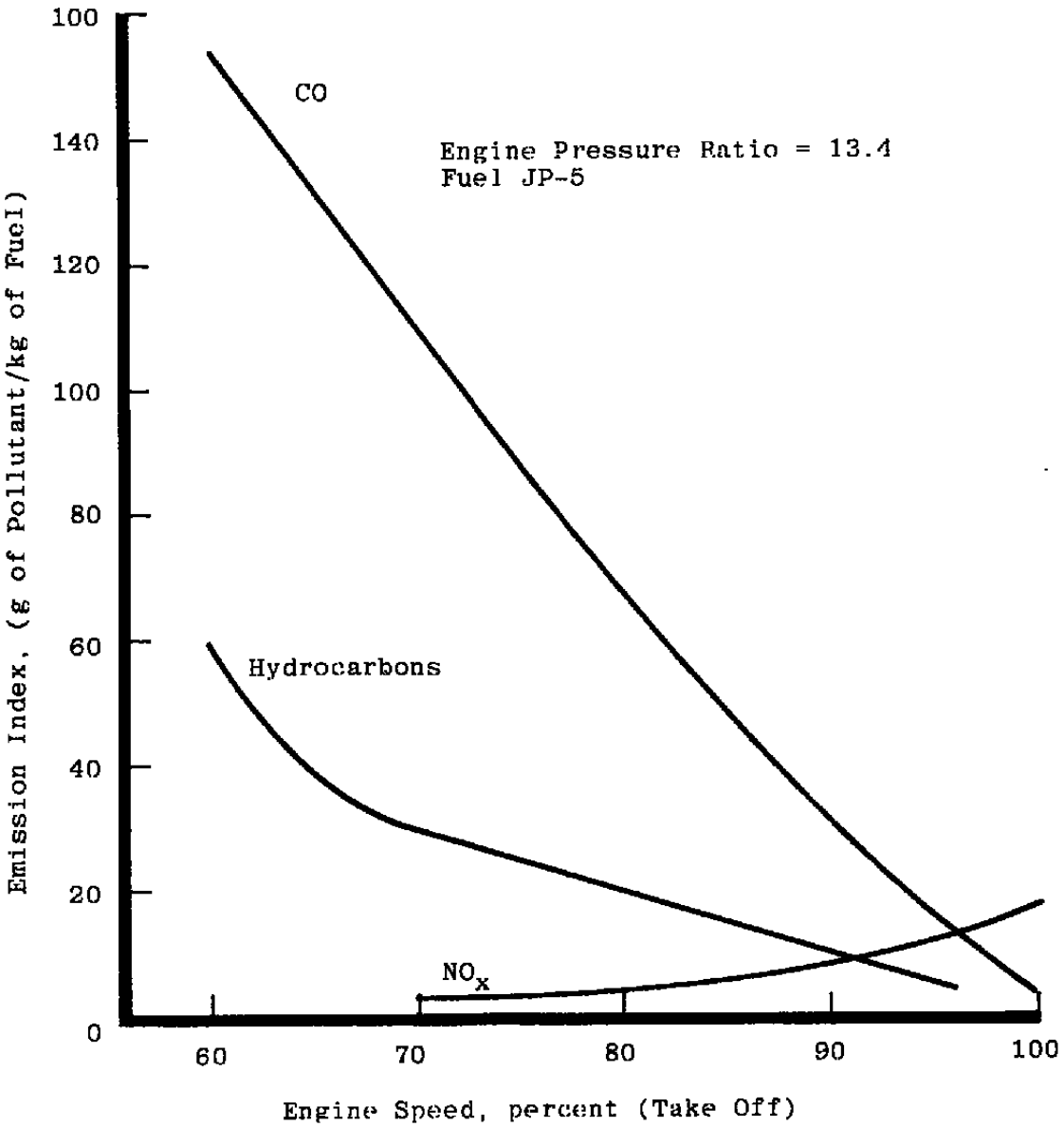


**Figure A-1. Typical engine enhaust emission characteristics (Ref. 18).**

fuel-air ratios in the reaction zone. The afterburner has a lower combustion efficiency than the main combuster and the products of incomplete combustion are estimated to be several times higher than from the main combustor (Ref. 18).

**Table A-1. Range of Turbine Engine Exhaust Constituents During Cruise Conditions**

| Constituents | Source | Estimated Concentration, percent |
|---|---|---|
| $N_2$ | Air | 76 (vol.) |
| $O_2$ | Air | 16.6 (vol.) |
| A | Air | 0.9 (vol.) |
| $H_2O$ | EFF Combustion | 2.7 (vol.) |
| $CO_2$ | EFF Combustion | 2.8 (vol.) |
| CO | INEFF Combustion | 10-50 ppm |
| Unburned HC | INEFF Combustion | 5-25 ppmC |
| Partially Oxidized HC | INEFF Combustion | 5-25 ppmC |
| $H_2$ | INEFF Combustion | 5-50 ppm |
| Smoke | INEFF Combustion | 0.4-50 ppm (mass) |
| NO, $NO_2$ | Heating of Air | 50-400 ppm |
| $SO_2$, $SO_3$ | Fuel | 1-10 ppm |
| Trace Metals | Fuel | 5-20 ppb |

## 2.0 MEASUREMENT OF EMISSIONS FROM A J85-GE-5 ENGINE

A program was conducted in the Engine Test Facility (ETF) at the Arnold Engineering Development Center (AEDC) to develop a mobile, self-contained gaseous and solid particulate emissions measurement system to define the exhaust emissions field of a typical turbojet engine. A production J85-GE-5 engine was used during this investigation. The testing was conducted at the ETF Ground Level Test Stand (Ref. 19).

Five species were measured in this study: hydrocarbons (CxHy), carbon monoxide (CO), carbon dioxide ($CO_2$), nitrogen dioxide ($NO_2$), and other oxides of nitrogen ($NO_x$). Of these species only the hydrocarbon results will be presented here.

The hydrocarbons in the exhaust products were measured with a Beckman Model 400 flame ionization detector (FID). Only total hydrocarbon concentration was measured and was expressed as methane equivalent.

Table A-2 gives the estimated performance parameters for the J85-GE-5 engine at the power levels used in this test. The inlet pressure was 14.2 psia and the inlet temperature was 59°F.

Data were taken on the engine centerline at nozzle exit and 16-ft aft of the nozzle exit for power levels of idle, cruise, military, and afterburner. The results of these measurements are

## Table A-2. J85-GE-5 Estimated Performance Parameters (14.2 psia and 59°F Inlet Conditions)

| Nominal Power Level | Engine Airflow, lbm/sec | Thrust / Thrust at Military × 100 | Engine Speed, N, percent Rated | Fuel Flow, lbm/hr | | Exhaust Gas Temperature, EGT, °R | Calculated Turbine Inlet Temperature, °R (Ref. 3) | Time Limit of Power |
|---|---|---|---|---|---|---|---|---|
| | | | | Engine | A/B | | | |
| Idle | 12.5 | 3.0 percent | 50.0 | 650 | — | 1,460 | — | Continuous |
| Cruise[1] | 37.6 | 59.0 percent | 95.0 | 1,800 | — | 1,610 | 1,785 | Continuous[1] |
| Military | 42.5 | 100.0 percent | 100.0 | 2,650 | — | 1,710 | 2,150 | 30 min |
| Minimum A/B | 42.5 | 112.0 percent | 100.0 | 2,650 | 1,000 | — | 2,150 | —[2] |
| Middle A/B | 42.5 | 128.0 percent | 100.0 | 2,650 | 2,950 | — | 2,145 | —[2] |
| Maximum A/B | 42.5 | 150.0 percent | 100.0 | 2,650 | 4,050 | ~3,300[3] | 2,140 | 5 min |

1 Maximum Power for Continuous Operation
2 Not Specified
3 Nozzle Discharge Temperature
4 Thrust at Military Power with Inlet Temperature of 519°R is Approximately 2,450 lbf

shown in Fig. A-2. The hydrocarbon emissions ranged from 10 ppmv at 16 ft with maximum afterburner to 6,600 ppmv at nozzle exit and mid-afterburner power. The emissions tend to be minimal at cruise and maximum afterburner. Data were also taken as a function of radial position at the exit plane of the engine and at the various power levels. The emission profiles are shown in Fig. A-3. The hydrocarbon emissions are largest at idle and minimum afterburner.

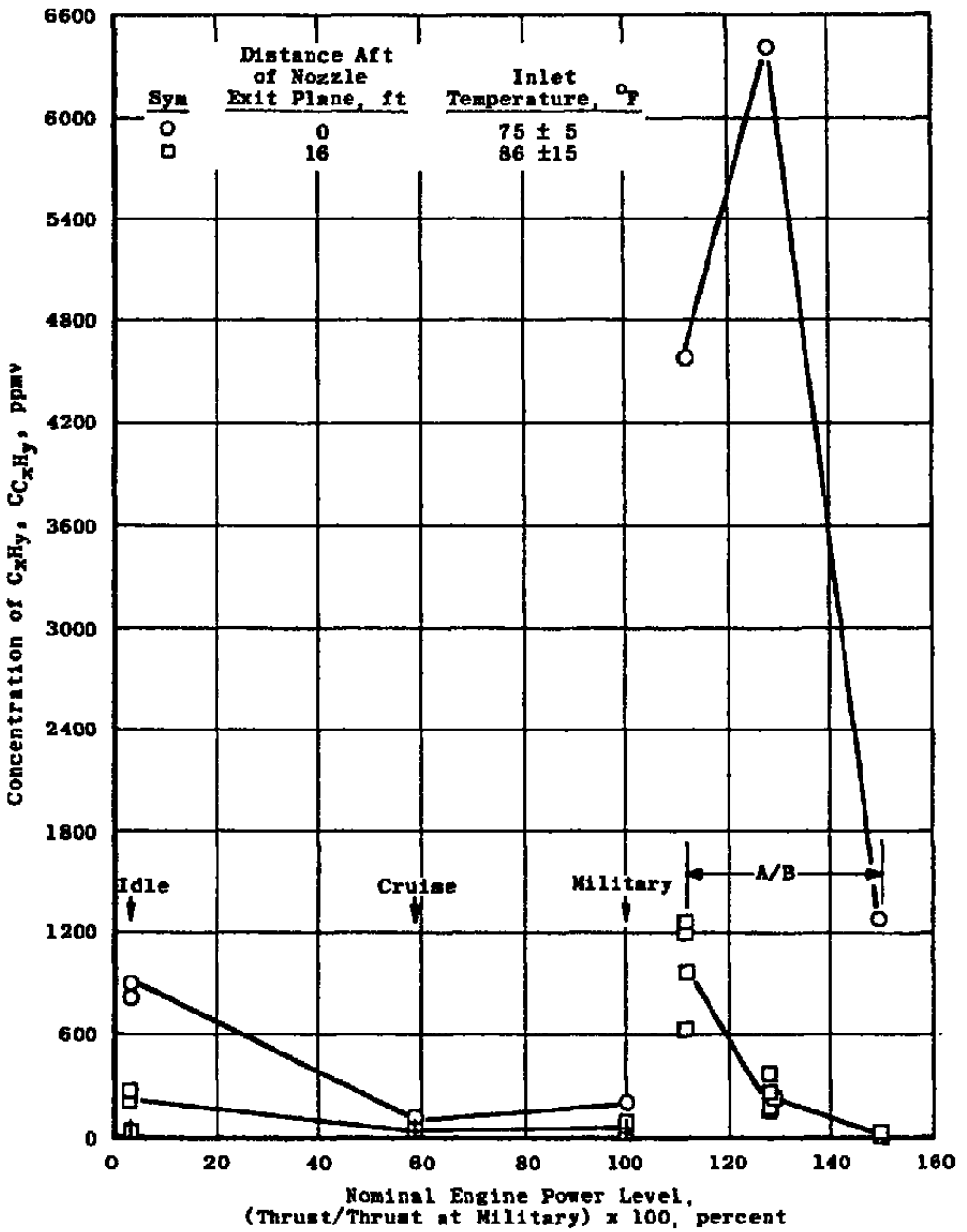


**Figure A-2. Pollutant concentration as a function of engine power level.**

This study showed that the hydrocarbon emission concentration decreased with increasing power at nonafterburning power levels. In afterburner operation the hydrocarbon emission concentration was a maximum for minimum afterburning.

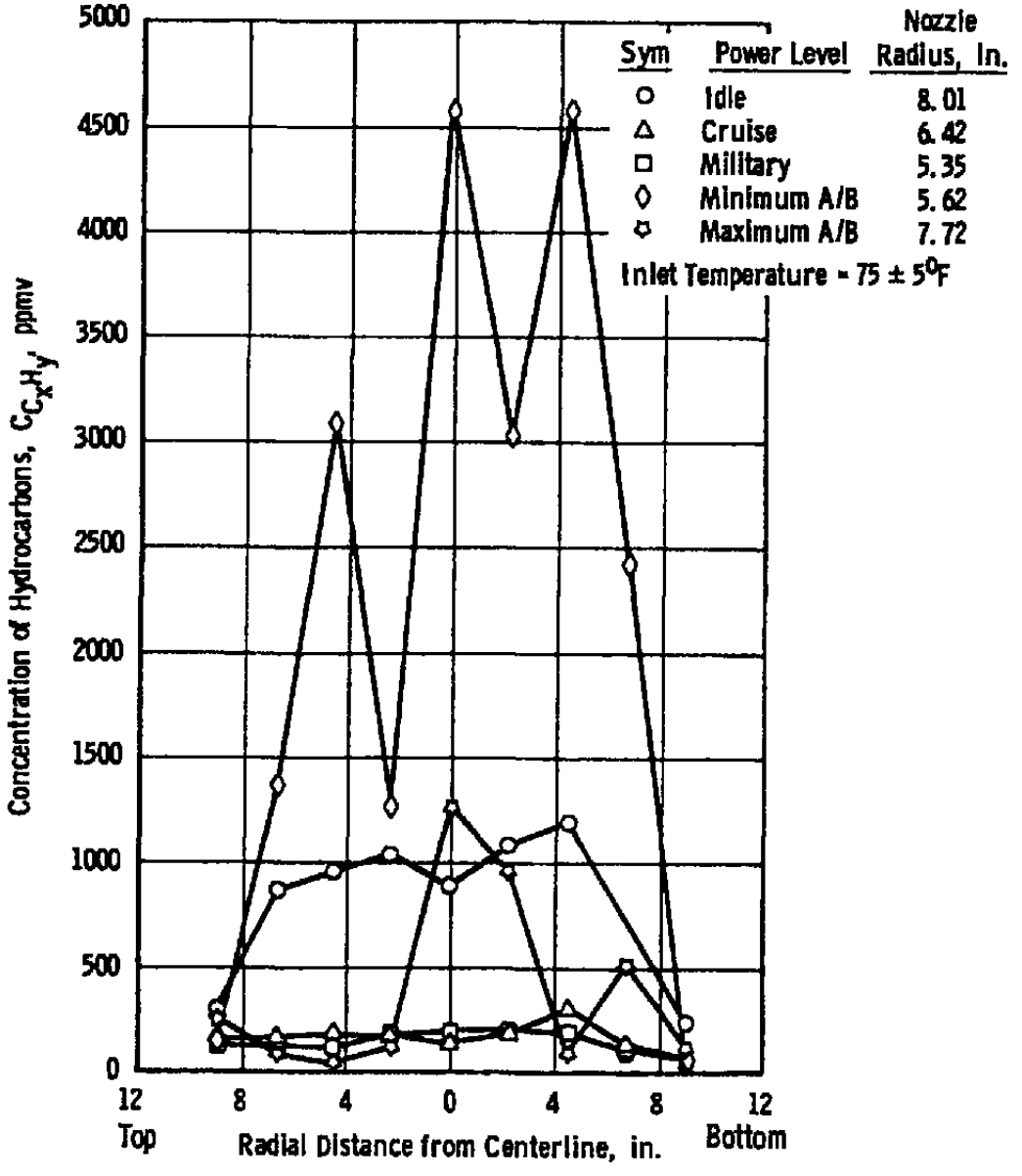


**Figure A-3. Effects of power level on the radial distribution of pollutant concentration at the nozzle exit.**

## 3.0 EMISSIONS STUDY AT SIMULATED ALTITUDE CONDITIONS

An emissions study was conducted on a YJ93-GE-3 engine in the Propulsion Engine Development Test Cell (J-2) at AEDC (Ref. 20). Operating conditions from take off to high-altitude supersonic cruise were used to determine the exhaust emissions from an SST-type engine. Emission data were obtained at simulated flight conditions from sea-level-static to Mach 2.0 at 75,000 ft and Mach 2.6 at 65,000 ft. Both afterburning and nonafterburning engine power settings were included. The emission measurements were taken at the engine nozzle exit. JP-5 fuel was used for the test program.

Table A-3 shows the unburned hydrocarbon emission index as a function of power setting for the various Mach numbers and altitudes studied. This same data are also shown in Fig. A-4. In addition to the online analysis, gas samples were taken and analyzed by the Bureau of Mines for some conditions. The results of their analysis are shown in Table A-4.

The results of this study agree with the results from the ground level test. That is, the emission indices for CxHy decrease with increasing power level from idle up through military power level. The emission increases for minimum afterburner and then decreases again for maximum afterburner.

## 4.0 LABORATORY COMBUSTOR RIG MEASUREMENTS

A recent laboratory study by Battelle, Columbus Laboratories (BCL) (Ref. 21) reports the measurement of many specific hydrocarbons. The instruments used were a gas chromatograph and flame ionization detector. The combustor rig was a one-sixth sector of the annular combustor from a G.E. TF-39 engine. JP-5 fuel was used and the tests were conducted with the combustor at idle fuel - air ratio. The results of test 14 which were typical of the study will be presented here.

Table A-5 (Ref. 21) gives the quantitative data from test 14. This table shows that ethylene is by far the most abundant species, with propane and acetylene also being major species. The results of test 14 for the various sampling and analysis methods are presented in Table A-6. From this data one would expect the concentration of methane in the exhaust of a turbine engine operating at idle condition to be approximately 10 parts per million. Table A-7 gives the breakdown of hydrocarbon species in exhausts by the number of carbon atoms in the molecules, up to C17.

**Table A-3. J93 Exhaust Emission Data**

| M | h, ft | $\phi$ | $\phi_m$ | Emission Index, lbm/1,000 lbm Fuel | | | |
|---|---|---|---|---|---|---|---|
| | | | | CO | $C_xH_y$ | NO (as $NO_2$) | $NO_x$ (as $NO_2$) |
| 0 | 0 | 0.123 | 0.114 | 122.00 | 45.300 | 0.66 | 0.21 |
| ↓ | ↓ | 0.113 | 0.105 | 111.00 | 28.100 | 1.42 | 2.73 |
| | | 0.112 | 0.101 | 94.40 | 17.400 | 1.72 | 3.11 |
| | | 0.123 | 0.114 | 66.00 | 7.270 | 1.81 | 3.54 |
| | | 0.163 | 0.163 | 38.80 | 1.980 | 2.13 | 4.72 |
| | | 0.237 | 0.231 | 26.30 | 1.260 | 2.80 | 5.27 |
| | | 0.325* | 0.315 | 7.58 | 0.030 | 4.93 | 5.78 |
| ↓ | ↓ | 0.448 | 0.482 | 9.78 | 0.076 | 3.09 | 3.82 |
| 0 | 0 | 0.560 | 0.649 | 1.34 | 0.058 | 3.44 | 3.61 |
| 0.8 | 20,000 | 0.331* | 0.341 | 6.49 | 0.068 | 4.82 | 5.12 |
| | ↓ | 0.454 | 0.521 | 5.01 | 0.071 | 3.57 | 3.59 |
| 0.8 | 20,000 | 0.546 | 0.670 | 1.64 | 0.027 | 3.40 | 3.36 |
| 0.9 | 36,000 | 0.331* | 0.312 | 18.90 | 0.117 | 3.42 | 3.99 |
| 1.4 | 35,000 | 0.226 | 0.222 | 19.10 | 1.480 | 1.88 | 3.91 |
| ↓ | ↓ | 0.318* | 0.321 | 7.82 | 0.169 | 4.23 | 4.60 |
| | | 0.436 | 0.478 | 37.60 | 1.780 | 1.63 | 2.95 |
| | | 0.528 | 0.626 | 4.61 | 0.054 | 2.40 | 2.70 |
| ↓ | ↓ | 0.613 | 0.723 | 3.24 | 0.031 | 2.61 | 2.90 |
| 1.4 | 35,000 | 0.713 | 0.843 | 3.33 | --- | 2.76 | 2.98 |
| 2.0 | 55,000 | 0.257 | 0.268 | 8.36 | 0.818 | 5.21 | 6.49 |
| ↓ | ↓ | 0.294* | 0.294 | 4.12 | 0.077 | 6.04 | 6.70 |
| | | 0.521 | 0.593 | 11.43 | 0.080 | 3.22 | 3.61 |
| | | 0.590 | 0.682 | 7.32 | 0.039 | 3.07 | 3.79 |
| 2.0 | 55,000 | 0.659 | 0.799 | 11.12 | 0.049 | 3.40 | 3.72 |
| 2.0 | 65,000 | 0.289* | 0.282 | 10.00 | 0.291 | 5.05 | 5.50 |
| 2.0 | 65,000 | 0.575 | 0.642 | 14.00 | 0.336 | 2.58 | 2.97 |
| 2.0 | 75,000 | 0.290* | 0.290 | 13.70 | 0.262 | 3.82 | 3.76 |
| 2.0 | 75,000 | 0.586 | 0.634 | 38.70 | 0.130 | 1.83 | 1.81 |
| 2.6 | 65,000 | 0.223* | 0.225 | 3.41 | 0.175 | 10.69 | 12.03 |
| 2.6 | 65,000 | 0.560 | 0.742 | 5.50 | 0.036 | 4.57 | 5.46 |

* Military Power

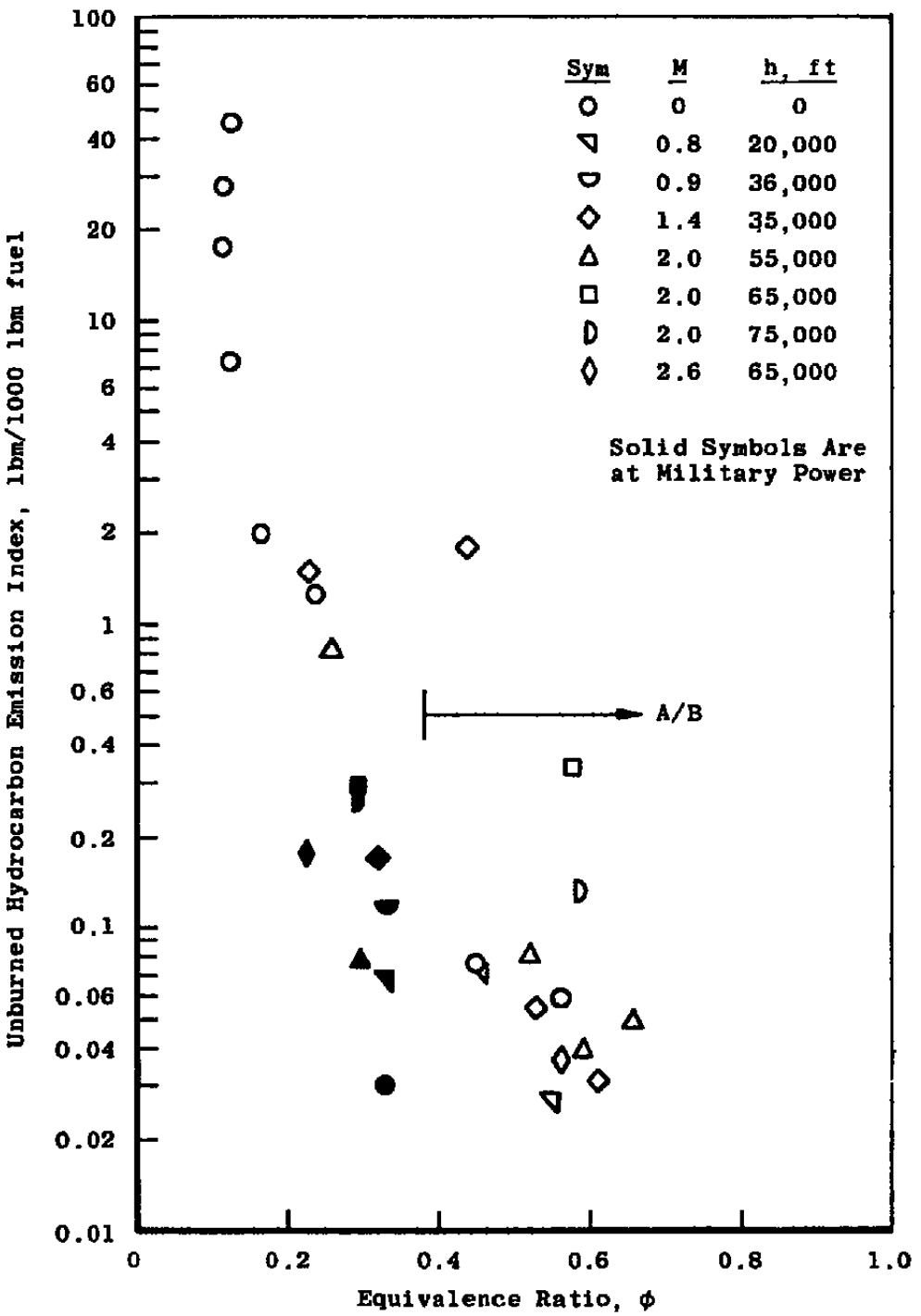


**Figure A-4. J93 Hydrocarbon exhaust emissions.**

**Table A-4. J93 Exhaust Gas Analysis**

| | | | | | | |
|---|---|---|---|---|---|---|
| M | 2.0 | 2.0 | 2.0 | 2.0 | 2.6 | 2.6 |
| h, ft | 65,000 | 65,000 | 75,000 | 75,000 | 65,000 | 65,000 |
| $\phi$ | 0.289 | 0.575 | 0.290 | 0.586 | 0.223 | 0.560 |
| Analysis* (Ref. 11): | | | | | | |
| $O_2$, percent | 15.0 | 8.6 | 15.2 | 10.8 | 17.8 | 9.8 |
| $CO_2$, percent | 3.6 | 8.9 | 3.7 | 5.9 | 2.7 | 9.0 |
| CO, ppmv | 156 | 673 | 260 | 1,860 | 35 | 220 |
| $H_2$, ppmv | 1.5 | 42.7 | 3.2 | 114.6 | 0.9 | 7.7 |
| $CH_4$, ppmC | 0.2 | 0.2 | 0.5 | 0.5 | 0.5 | 0.5 |
| $C_xH_y$, ppmC | 16.6 | 53.4 | 18.0 | 20.0 | 34.5 | 43.9 |
| Total Aldehyde, ppmv | 0.56 | 1.49 | 1.96 | 4.10 | 0.24 | 0.18 |
| Formaldehyde, ppmv | 0.53 | 0.89 | 0.25 | 0.42 | 0.02 | 0.17 |
| $H_2O_2$, ppmv | --- | --- | --- | --- | --- | --- |
| $N_2O$, ppmv | 1.98 | 1.57 | 1.45 | 0.78 | 1.23 | 2.26 |
| NO, ppmv | 2.25 | 2.20 | 0.86 | 2.13 | 1.63 | 2.33 |
| $NO_x$, ppmv | 4.88 | 2.20 | 1.70 | 3.20 | 3.00 | 3.23 |
| Nitrate, ppmv | 6.7 | 5.0 | 3.2 | 1.6 | 7.5 | 1.5 |
| Nitrate, ppmv | 62.4 | 71.9 | 44.8 | 38.2 | 72.2 | 132.6 |

* Dash indicates not detectable, below 0.01 ppm

**Table A-5. Major Species Quantified by the Cryogenic Sampling Technique, (Ref. 21)**

| Compound [ppmC] | Test 14 |
|---|---|
| 1. Ethane | 2.21 |
| 2. Ethylene | 77.80 |
| 3. Propane | 0.75 |
| 4. Acetylene | 18.61 |
| 5. Propene | 26.52 |
| 6. Acetaldehyde | 1.83 |
| 7. 1-Butene | 5.83 |
| 8. 1,3-Butadiene | 11.13 |
| 9. $C_4$-ene | 7.60 |
| 10. C-2-Butene | 1.31 |
| 11. 2-Propenal (Acrolein) | 7.42 |
| 12. Acetone | 3.43 |
| 13. 1-Pentene | 5.01 |
| 14. N-Pentane | 1.18 |
| 15. $C_5$-ene | 3.14 |
| 16. 2-Methyl1-2-Butene | 1.26 |
| 17. $C_5$-ene | 1.94 |
| 18. 2-Methyl-2-Propenal (or Crotonaldehyde) | 2.79 |
| 19. 2-Methylpentane | 1.35 |
| 20. 1-Hexene | 4.98 |
| 21. Benzene | 9.07 |
| 22. 1-Heptene | 3.16 |
| 23. N-Heptane | 0.44 |
| 24. Toluene | 3.33 |
| 25. Hexanal | 1.09 |
| 26. 1-Octene | 2.13 |
| 27. N-Octane | 0.63 |
| 28. Ethylbenzene | 1.33 |
| 29. M + P-Xylene | 1.70 |
| 30. Styrene | 2.01 |
| 31. O-Xylene | 1.06 |
| 32. 1-Nonene | 1.91 |
| 33. N-Nonane | 0.99 |
| 34. Benzaldehyde | 2.12 |
| 35. N-Decane | 2.00 |
| 36. N-Undecane | 8.05 |
| 37. Napthalene | 3.52 |

**Table A-6. Summary of Organic Species Meassured by Various Sampling and Analysis Methods for Test No. 14, ppmC (Ref. 21)**

| | |
|---|---|
| $CH_4$ (G.C.-F.I.D.) | 9.6 |
| $C_2$ through $C_9$ (Cryogenic)[a] | 285 |
| $C_{10}$ through $C_{17}$ (XAD-2) | 165 |
| PAH (3+ rings)[b] | < 0.01 |
| Aldehydes (DNPH) | 31.6 |
| Total Organics by Species Summation | 491 |
| Total Organics by Continuous F.I.D. Method | 525 |

(a) Cryogenic data excludes aldehyde species.
(b) PAH analyses were completed for select tests.

**Table A-7. Total Organic Species Contribution by Carbon Number, (Ref. 21)**

| Compound | ppmC |
|---|---|
| $C_1$ to $C_2$ | 19.8 |
| $C_2$ to $C_3$ | 124.7 |
| $C_3$ to C4 | 44.9 |
| $C_4$ to $C_5$ | 47.4 |
| $C_5$ to $C_6$ | 24.7 |
| $C_6$ to $C_7$ | 22.2 |
| $C_7$ to $C_8$ | 14.2 |
| $C_8$ to $C_9$ | 14.4 |
| $C_9$ to $C_{10}$ | 13.7 |
| $C_{10}$ to $C_{11}$ | 16.3 |
| $C_{11}$ to $C_{12}$ | 33.6 |
| $C_{12}$ to $C_{13}$ | 35.9 |
| $C_{13}$ to $C_{14}$ | 33.6 |
| $C_{14}$ to $C_{15}$ | 22.7 |
| $C_{15}$ to $C_{16}$ | 12.6 |
| $C_{16}$ to $C_{17}$ | 7.1 |
| $C_{17}$ and above | 2.9 |
| Total Organics | 490.7 |

## 5.0 FULL-SCALE ENGINE EMISSIONS MEASUREMENTS BY BATTELLE

In a continuation of the measurement program discussed in Section 4.0, Battelle, Columbus Laboratories made gaseous emission measurements on two engines in current use (Ref. 22). A General Electric TF-39 engine, currently in service on the U. S. Air Force Lockheed C-5 aircraft, was used in the study. Gaseous emissions control was not a significant design factor in the TF-39 engine. Therefore, the TF-39 engine does not meet the EPA or ICAO gaseous emissions standards.

The other engine used in the study was a CFM-56 engine, which is representative of the latest technology in fuel efficient engines with advanced emission control features. The CFM-56-2 is used on the Air Force KC 135 tankers as well as on McDonnell Douglas DC-8 Series 70 commercial transports. The CFM-56-3 is scheduled for use on the Boeing 737-300. The core engine of the Air Force F101 engine for the B-1B bomber is essentially a CFM-56 engine.

The turbine engine emissions tests were conducted at the General Electric Peebles Test Operation. The Peebles Test Facility is an outside ground-level test facility. Table A-8 gives the variables measured in the test, as well as the techniques and instruments used to accomplish the measurements.

The sampling rake was mounted behind the engine and consisted of four equally-spaced arms which extended radially outward from centerline. Each arm had sampling ports at 1-in. intervals from 6 to 17 in. from center. All sampling ports were connected so that a single sample was collected.

The tests were conducted with JP-4, JP-5, and JP-8 fuels at power settings of idle, 30-percent and 80-percent power. The results are consistent with the earlier studies in that the total hydrocarbon concentration decreases with increasing power level and combustion efficiency. Also the total hydrocarbon levels are significantly less with the CFM-56 engine than with the TF-39 engine.

Table A-9 summarizes the results for the TF-39 engine and CFM-56 engine tests for the major constituents using JP-5 fuel. Methane, ethylene, acetylene, propane, and benzene appear to be major constituents of the hydrocarbons. The average concentration of each species in ppmc is presented for each engine and power level. Although many species were identified in the measurements, only the major ones are presented here.

The same species are present in the exhaust from both engines. Also the relative abundance of each species appears to be approximately the same for both engines. However, the individual concentrations of each species are significantly lower with the CFM-56 engine which is consistent with the total hydrocarbon measurement.

## 6.0 SUMMARY OF SURVEY RESULTS

The results of past hydrocarbon emission studies performed on the exhaust from turbine engines are very consistent on the relations between hydrocarbon concentration and engine operating conditions. The main points to be found in these reports are as follows:

1. The hydrocarbon concentration in the exhaust for nonafterburning operation is highest for idle and decreases with increasing power to military power level.

2. In afterburner operation the hydrocarbon concentration increases sharply, with the maximum occurring at some intermediate afterburner power level, and then decreases at maximum afterburner power level.

3. In measurements downstream from the nozzle exit, the trends are the same but with lower hydrocarbon concentrations, except for afterburner operation, where the maximum concentration occurs at minimum afterburn rather than intermediate.

4. At simulated altitude and Mach number in test cell operation, the trends remain the same as for ground-level testing, but the concentration decreases with altitude.

5. When specific hydrocarbon concentrations were measured, the major species were methane, ethylene, acetylene, propane, 1-butene, n-hexane, benzene, 2-methylhexane, 3-methylhexane, and n-heptane. Methane generally appears to make up about 2 - 4 percent of the total hydrocarbons.

6. The specific hydrocarbon concentrations tend to decrease with increasing power level in nonafterburner operation, which is consistent with total hydrocarbon measurements.

**Table A-8. Variables Measured During the Emission Experiments**

| Variable | Technique | Instrument |
|---|---|---|
| **General Electric** | | |
| $NO/NO_x$ | Chemiluminescence | Beckman 951 |
| CO | Nondispersive Infrared | Beckman 865 |
| $CO_2$ | Nondispersive Infrared | Beckman 864 |
| THC | Flame Ionization | Beckman 402 |
| **Battele** | | |
| Methane | Canister Samples/Flame Ionization GC | Beckman 6800 |
| CO | Canister Samples/Flame Ionization GC | Beckman 6800 |
| $C_2$ to $C_{10}$ Organics | On-Line Flame Ionization GC | Hewlett-Packard 5880 |
| $C_{10}$ to $C_{17}$ Organics | XAD-2/Flame Ionization GC | Hewlett-Packard 5730 |
| PNA Compounds | XAD-2/Gas Chromatography/Mass Spectrometery | Finnigan 4000 |
| Aldehydes | DNPH Derivatization/HPLC | With LDC Spectro Monitor III UV Detector |
| THC | Flame Ionization | Beckman 402 |

**Table A-9. Summary of Results for Jet Engine Operating With JP-5 Fuel**

| Compound (ppmC) | TF 39 Engine | | | CFM 56 Engine | | |
|---|---|---|---|---|---|---|
| | Idle | 30-percent Thrust | 80-percent Thrust | Idle | 30-percent Thrust | 80-percent Thrust |
| Methane | 9.42 | 1.63 | 1.09 | 5.83 | 0.58 | 0.44 |
| Ethylene | 62.28 | 3.03 | 0.04 | 35.25 | ND | 0.05 |
| Acetylene | 16.85 | 1.23 | ND | 9.67 | ND | ND |
| Propene | 21.33 | 0.42 | 0.02 | 10.34 | 0.01 | ND |
| Benzene | 7.45 | 0.49 | 0.03 | 4.13 | 0.02 | 0.02 |
| THC (ppm) | 349.5 | 14.7 | 4.2 | 174.6 | 3.1 | 5.2 |